

A noninvasive optical probe for breast cancer: diagnostic use of acoustically induced blood stasis

B.A. Winey*^a, V. Misic^b, B. Fenton^b, L. Liao^c, K. Parker^d, Y. Yu^b

^aDept. of Physics and Astronomy, University of Rochester, Rochester, NY 14627

^bDept. of Radiation Oncology, University of Rochester Medical Center, Rochester, NY 14642

^cDept. of Imaging Sciences, University of Rochester Medical Center, Rochester, NY 14642

^dSchool of Engineering and Applied Sciences, University of Rochester, Rochester, NY 14627

ABSTRACT

Ultrasound-induced blood stasis was demonstrated thirty years ago. Most of the literature has been focused on methods employed to prevent stasis from occurring during ultrasound imaging. The current work discusses some of the theory behind this phenomenon. It also demonstrates ultrasound-induced blood stasis in murine tumor and muscle tissue, observed through noninvasive measurements of optical spectroscopy, and discusses possible diagnostic uses. We demonstrate that, using optical spectroscopy, effects of ultrasound can be used to noninvasively differentiate tumor from muscle tissue in mice, and that we can quantitatively differentiate tumor from muscle with maximum specificity 0.83, maximum sensitivity 0.79, and area under ROC curve 0.90, using a simple algorithm.

Keywords: Tissue diagnosis, novel use of ultrasound and spectroscopy

1. Introduction

Stationary sound waves have long been known to create banding effects when solid particles are suspended in liquids; sand in air (in a cylinder), bubbles in water, etc. In 1971, Dyson et. al. reported that stationary ultrasound waves can create bands of red blood cells *in vivo*, using chick embryos removed from the egg shell but kept alive in saline solution¹. Later, ter Haar and Wyard reported that the banding was due to the standing pressure wave created by the ultrasound². Nyborg derived that even a traveling pressure wave, with small amounts of reflection at the tissue boundaries, can cause banding of blood cells in the plasma medium³. Many have continued to study the diagnostic limits and dangers of ultrasound and ultrasound-induced stasis⁴⁻⁷, but to the best of our knowledge, no one has investigated the diagnostic potential.

It has been shown that oxy and deoxyhemoglobin have signature absorption and scattering effects visible in steady-state broadband diffuse reflectance optical spectroscopy⁸. Furthermore, oxyhemoglobin saturation can be determined using spectroscopic measurements of light reflected from tissue and analyzed with the diffusion approximation or the higher order P₃ approximation⁹⁻¹⁰.

As the cells consume oxygen, hemoglobin molecules in the blood continually replenish the oxygen supply as the blood flows through the vessels. When standing wave ultrasound is used to slow or stop the blood flow, the oxyhemoglobin saturation decreases as the available oxygen is depleted; the oxyhemoglobin saturation can be observed to decrease, using optical spectroscopy measurements, and return to relaxed levels shortly after the ultrasound radiation is stopped.

The current experiments combine focused standing wave ultrasound-induced blood stasis and optical spectroscopy to develop a noninvasive imaging tool with potential use in tissue diagnostics. In this paper we demonstrate that optical spectroscopy measurements of ultrasound induced blood stasis can be used to differentiate tissue type noninvasively.

2. Methodology

2.1 Theory

The current model of standing wave ultrasound interaction with blood cells detailed by ter Haar looks at the effects of a stationary acoustic pressure field on individual spherical, compressible spheres in a single dimension². The acoustic pressure field is assumed to obey the following equation:

$$F_{sw} = \frac{V_0 P_A^2}{4 \rho_0 c_0^2} k \sin 2kx \cdot f\left(\frac{\rho}{\rho_0}\right), \text{ where } f\left(\frac{\rho}{\rho_0}\right) = \left[\frac{\rho_0 c_0^2}{\rho c^2} - \left(\frac{5\rho - 2\rho_0}{3\rho + \rho_0} \right) \right] \quad (1)$$

and V_0 is the volume of the sphere, P_A is the amplitude of the acoustic pressure wave, ρ_0 and ρ are the densities of the fluid inside and outside the sphere, respectively, k is the wave number of the fluid and x is the dimension parallel to the direction of propagation. The formula was derived by Yosioka and Kawasima in 1955 for acoustic fields acting on compressible spheres without membranes suspended in a fluid, with specific consideration given for air bubbles in water¹². The time component of the acoustic field is averaged out of the integral solutions under consideration of periodic arguments.

2.2 Experiment Setup

Ultrasound was generated by a 1 MHz piezoelectric ceramic crystal (Channel Industries) mounted behind a concave aluminum lens with a focal length of 7 cm. At 1 MHz the -6 dB focal zone diameter was 2 mm and the focal zone length was 30 mm. The ultrasonic field was measured and characterized using a hydrophone (Onda Co. HNR 500) with spatial sensitivity of 0.5 mm. The hydrophone was calibrated with a steel ball technique. The intensity of the ultrasound was maintained at Spatial Peak Temporal Average Intensity (SPTA) $\approx 0.7 \text{ W/cm}^2$, averaged over the burst cycle. The current experiments were conducted within the FDA therapeutic ultrasound limits (SPTA = 0.720 W/cm^2) and blood stasis and banding have been observed to be reversible under these conditions.

All experiments were conducted in a Plexiglas water tank. Distilled water was autoclaved for 45 minutes to remove ions and micro-bubbles in order to prevent cavitation and scattering of the acoustic field. A 2.5 cm thick piece of aluminum was used for the acoustic reflector and a 2.5 cm thick rubber block was placed behind the aluminum to absorb any scattered acoustic energy. During experiments the water was heated to 37°C using a circulating water heater and the rubber block was positioned to shield the data collection area from most of the water currents since moving water can interfere with spectroscopy measurements (Fig. 1).

Diffuse reflectance spectra were collected with a single 600 micron fiber, numerical aperture (N.A.) = 0.22, residing at the center of a seven fiber probe (Ocean Optics, R600-7-VIS/NIR). The center collection fiber was connected to a 2048 pixel room temperature spectrometer (Ocean Optics, USB 2000-VIS/NIR) fitted with a grating for spectrum analysis between 200 nm and 1100 nm. The outer six fibers were connected to a broadband halogen light source (Ocean Optics, HL 2000). The source detector separation was 1 mm, resulting in an inspection volume of $\approx 9 \text{ mm}^3$, mostly within 1 mm of the tissue surface. The optical signal was weighted by the intensity curve of the light source. The intensity curvature was measured with a diffuse reflectance standard.

2.3 Experimental Procedure

Six-eight (6-8) week old C3H/HeJ mice were inoculated intramuscularly to the right thigh with 10^6 MCA-35 mammary carcinoma cells, with the left hind leg muscle tissue used as control for the diagnostic portion of this experiment. In order to deduce the experimental effects, two mice were inoculated to the left thigh with the right leg muscle tissue used as the control and the results were not affected. The mice were sedated using a Ketamine Xylazine mixture injected intraperitoneally and placed in a Plexiglas restraint which positioned the leg to be examined away from the body. The probe was then fixed on the skin of the mouse leg using a positioning arm, ensuring contact but without skin compression. During data collection, the probe was held stationary, maintaining a constant pressure on the mouse skin. Optical spectroscopy measurements of hemoglobin *in vivo* are highly dependent upon surface pressure since any changes will affect the blood/hemoglobin volumes. Once a baseline spectrum was achieved (≈ 4 minutes), the mouse and probe were moved such that the focus of the ultrasound was $\approx 2 \text{ mm}$ directly under the location of the optical probe. The

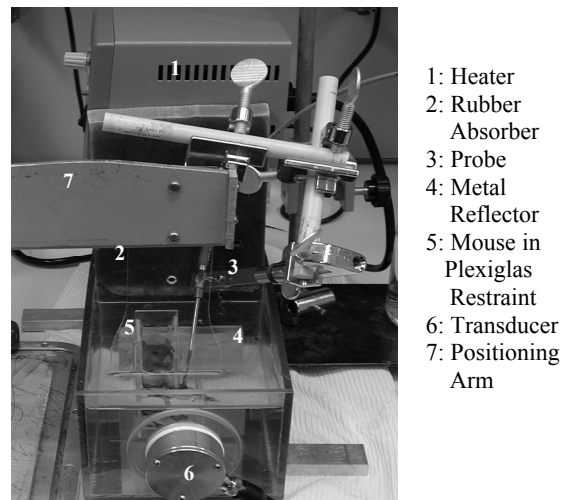


Fig. 1. Experimental setup, with the mouse leg located in the focal region of the ultrasound.

direction of propagation of the ultrasound and light were kept orthogonal so that the metallic probe did not enter the focus of the ultrasound and obstruct or scatter the standing acoustic wave. Also, this increased the probability of intersecting the acoustic focal region with the volume of optical inspection.

During each experiment, ultrasound was administered in 5 second bursts, with 55 second relaxation periods between bursts and a total of six bursts per leg per experimental collection. For each mouse, both legs, one with a tumor (diameter ≈ 10 mm) and one without, were subjected to ultrasound and optical spectroscopy to compare the effects in tumor versus nontumor tissue. The order of inspection of the legs was altered to diminish the possibility that the results were influenced by the depth of the anesthesia, which can directly affect the blood velocity.

Ultrasound pulse information for each experiment was monitored and collected with the oscilloscope and stored for later signal correlation studies. Optical spectra were collected with the supplied Ocean Optics software at 500 ms intervals in order to decrease the Signal to Noise Ratio (SNR) and to reduce the appearance of unwanted higher frequency signals and noise.

The raw optical spectra were corrected for the curvature of the light source intensity. The intensity curve of the light source was obtained using a diffuse reflectance standard. The optical signal then was cropped to avoid the spectral regions of low light (< 400 nm) and regions near the end of the spectrometer's sensitivity (> 1000 nm). Ultimately, the spectra were cropped to regions between 475 nm and 650 nm where significant optical absorption occurs due to oxy/deoxyhemoglobin presence, especially in short (≈ 1 mm) source detector separation configurations, and few other absorbers (i.e. water) exert significant effects.

The spectra were analyzed using a P_3 approximation method detailed in Refs. 10 and 11 to gather oxy/deoxyhemoglobin concentrations, as well as scattering information, before, during, and after ultrasound pulses. In addition to the P_3 fitting algorithm, several isolated wavelengths were initially considered (515, 528, 540, 560, 579, and 578 nm), due to the characteristic effects of oxy/deoxyhemoglobin shifts at these points, but ultimately the ratio of intensities (I) at two wavelengths, 560 nm and 540 nm, was chosen. The ratio of I_{560}/I_{540} was observed to be significantly affected by the presence (or absence) of the ultrasound. The intensities at 560 nm and 540 nm are dependent upon the oxy/deoxyhemoglobin saturations, at 560 (540) nm the reflected signal increases (decreases) as the oxyhemoglobin concentration increases.

2.4 Immunohistochemistry and image analysis of vascular spacing and area

To visualize blood vessels open to flow, an *i.v.* injected stain, DiOC₇, was injected 1 min prior to tumor freezing, which preferentially stains cells immediately adjacent to the vessels¹³. Tumor sections were imaged using a 20 \times objective, digitized, background-corrected, and analyzed using Image-Pro software¹³. Color images were acquired and digitally combined under two staining conditions. First, images of the DiOC₇ were obtained immediately after cryostat sectioning. Following staining, the sections were returned to the same stage coordinates, and anti-panendothelial antigen (Pharmingen, San Diego, CA) images were acquired to mark total anatomical vessel locations. Vessels were quantified using automated image analysis techniques¹⁴. Briefly, distance map filters converted pixel intensities of the vessel images to intensity levels proportional to the distances between tumor cells and the nearest vessels. This distance map was multiplied by an image of white grid points on a black background to obtain a spatial sampling of the distance map intensities, which are proportional to the distances to the nearest vessel (vessel spacing).

3. Results

3.1 Tests of the Experimental Setup

Initial tests of our ultrasound setup included a repeat of Dyson's seminal experiment¹, but with lower acoustic intensities (SPTA = 0.7 W/cm²) and lower frequencies ($f \approx 1$ MHz). The ultrasound was observed visually to stop blood flow in the chick embryo vessels, causing bands to form for short periods of time (data not shown). The bands were observed to form at half wavelength separations.

In order to perform a non-invasive test regarding the efficacy of the ultrasound in the mouse leg, a laser Doppler system (Transonic BLF21) was used to verify blood flow slowing or stasis due to ultrasound in the healthy leg muscle and the

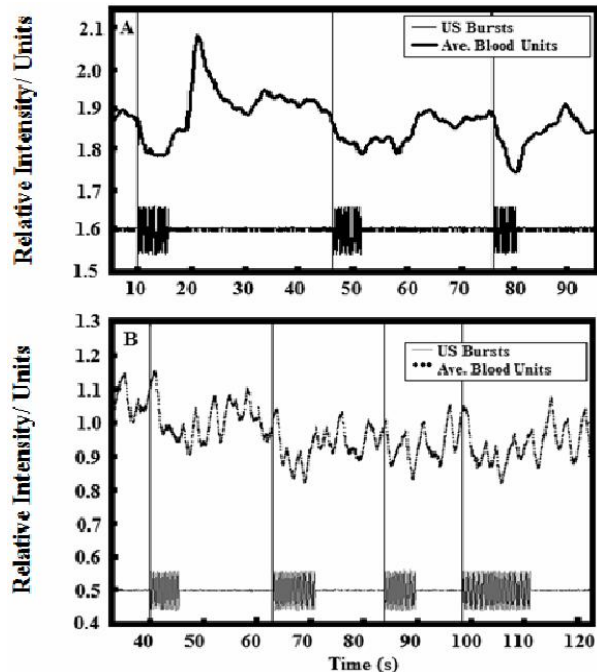


Fig 2. Laser Doppler relative average volume velocity shown with ultrasound bursts and vertical lines for reference for normal leg muscle (a) and tumor (b) tissue samples. The normal leg muscle samples have greater blood volume flow rates.

tumor tissue. From the laser Doppler measurements, it was clear that in a small target volume of healthy tissue average velocity of the blood was slowing (Fig. 2a.), but there was no noticeable effect in the tumor tissue (Fig 2b.). The vertical lines denote when the ultrasound was introduced, with the ultrasound being turned off after 5 seconds. The large velocity peak in Fig. 2a following the tissue recovery after the first pulse is believed to be due to vessel dilation as the tissue responded to the oxygen deprivation. The laser Doppler probe had an observation depth of ≈ 1 mm and a volume of inspection of ≈ 1 mm³. When this same volume element was inspected with white light in the presence of ultrasound, there were measurable changes in the oxyhemoglobin saturation.

Before every experiment, the presence of standing wave ultrasound was visually confirmed using an interference technique. The density bands formed by standing wave ultrasound create an interference pattern when light passes through the tank. The location and intensity of the focal zone were also confirmed using the hydrophone between experiments.

3.2 *In Vivo* Diffuse Reflectance Optical Spectroscopy

Reflectance spectra obtained *in vivo* were collected from the center, 600 micron fiber of the seven fiber bundle with a separation of 1 mm from each source fiber. Complete spectra data (400-1100 nm) were stored for every experimental collection period (≈ 10 minutes/leg) at 500 ms intervals.

The complete spectra were analyzed with a technique similar to the one described by Finlay and Foster, which is applicable for small source detector separations¹¹. The P₃ fitting algorithm assumes that in a specific wavelength range (380-750 nm) the absorption spectrum is dominated by a linear combination of the absorption spectra of oxy- and deoxyhemoglobin. The absorption coefficients were taken from data compiled by Prahl¹⁵.

The hemoglobin concentrations, the scattering parameters, and the total hemoglobin concentrations for a complete collection period are given in

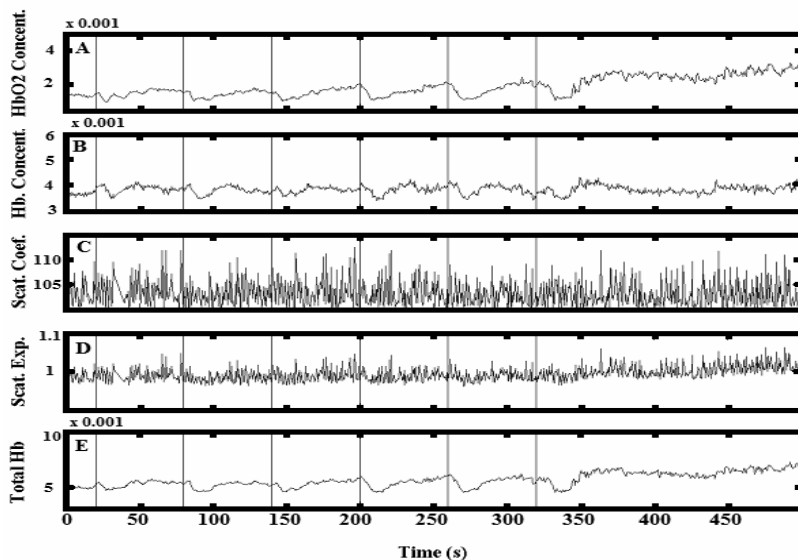


Fig. 3: Parameters derived using the P₃ fitting algorithm applied to the collected broadband diffuse reflectance spectra: (a.) oxyhemoglobin concentration, (b.) deoxyhemoglobin concentration, (c.) scattering coefficient, (d.) scattering exponent, and (e.) total hemoglobin concentration. The vertical lines reference the beginning of the five second bursts of ultrasound.

Fig. 3. The ultrasound was observed to have no correlated effect on the scattering properties of the tissue. The results displayed a large drop in oxyhemoglobin concentration when ultrasound is introduced. The deoxyhemoglobin, however, also displayed a drop in concentration. The drop was less significant and as a portion of the total hemoglobin, it actually increased. This seems to imply that the oxyhemoglobin was not only decreasing due to consumption without

replenishing but also due to a decrease in blood volume. This might be due to a squeezing of tissue due to the presence of the acoustic standing wave.

The calculation of these results from a complete collection period required thirteen hours of CPU time. In order to more efficiently estimate changes in tissue oxygenation, a technique known as oximetry was employed. Oximetry is a technique that uses a ratio of intensities at two or more wavelengths to measure tissue properties. Various commercial products use oximetry to measure hemoglobin saturation. Oximetry is generally insensitive to many physiological artifacts, such as scattering properties and blood volume, and, without calibration, is incapable of determining absolute oxy/deoxyhemoglobin concentrations. Oximetry was used because of its speed and ease of calculation and because it was observed to reflect the oxyhemoglobin dynamic changes.

It can be shown, using the P_3 fitting algorithm, that the ratio I_{560}/I_{540} correlates to oxyhemoglobin concentrations and that the ultrasound has no observable effect on the scattering properties of the tissue in the wavelength range considered. By visual comparison of the I_{560}/I_{540} signal with the ultrasound signal, one can generally establish temporal correlation between these two signals in the muscle scans and the absence of correlation in the tumor scans (Fig. 4a and 4b). The drops in the I_{560}/I_{540} ratio signal have been consistently observed in muscle scans and are mostly absent in tumor scans.

To demonstrate that it was possible to establish mathematical correlation between the I_{560}/I_{540} signal and the ultrasound signal, a simple computer algorithm was written¹⁶. The standard deviation of the cross-covariance of the ultrasound square pulse and the I_{560}/I_{540} signal was computed in order to provide a quick estimate of the degree of correlation. Repeatable large decreases in the oxyhemoglobin and the I_{560}/I_{540} signal corresponding to the timing of the ultrasound pulses produce the greatest degree of correlation. The trend of the I_{560}/I_{540} signal was subtracted from the ultrasound pulse data in order to decrease the effects of signal slope on the cross-covariance.

The standard deviation of the cross-covariance for each leg, tumor and muscle, and for each mouse, was calculated and compared to the opposite leg of the same mouse as a ratio. The ratios for twenty-four mice are presented in Fig. 5. The strength of the correlation is reflected in the height of the bar in Fig. 5. The ratio of the standard deviations was greater than 1 (one) in all but one experiment, and greater than 2 (two) in 75% of measured mice. A ratio greater than one means that the I_{560}/I_{540} signal of the nontumor leg is more correlated to the ultrasound signal than the I_{560}/I_{540} signal of the tumor tissue. In other words, a ratio great than one means that the “dips” in the I_{560}/I_{540} signal of the nontumor sample are deeper than the “dips” in the tumor sample.

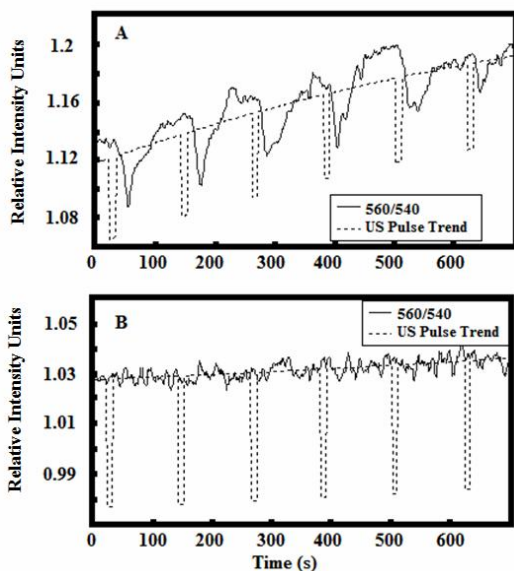


Fig. 4. The ratio I_{560}/I_{540} signal with the trend modulated ultrasound pulse signal superimposed for a typical (a) normal leg muscle tissue and (b) tumor tissue.

After demonstrating a large degree of correlation between I_{560}/I_{540} signal and the ultrasound pulse signal for nontumor tissue sample, a second computer algorithm¹⁶ was written with the aim of creating a diagnostic program based on an *in vivo* experimental observation.

The diagnostic algorithm applied a decision threshold to determine which measurements were gathered from tumor or muscle tissue samples. If the diagnostic value, $\{0,1\}$, corresponding to the “degree” of ultrasound- I_{560}/I_{540} signal correlation, was greater than the threshold, the sample was classified as a tumor. For a threshold value of zero, all tumor samples were labeled correctly, producing a perfect sensitivity of 1. But, this same threshold labeled 71% of the muscle samples as tumor, producing a specificity of 0.29. For a threshold of one, the algorithm labeled every sample as nontumor and generated a specificity of 1 but a sensitivity of 0. For clinical settings, sensitivity (high true-positives) and specificity (high true negatives) should be maximized simultaneously. The algorithm achieved the best results with the decision threshold 0.40; specificity was 83.3% and sensitivity was 79.2%. Complete results of this experiment are presented in Fig. 6.

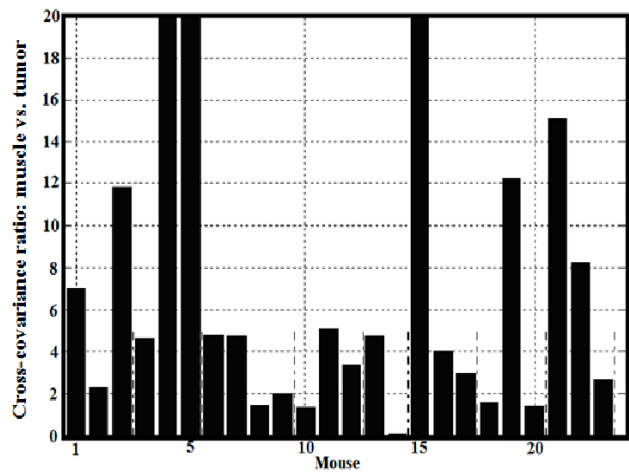


Fig. 5. The I_{560}/I_{540} correlation ratio signal which reflects the changes in oxyhemoglobin concentrations.

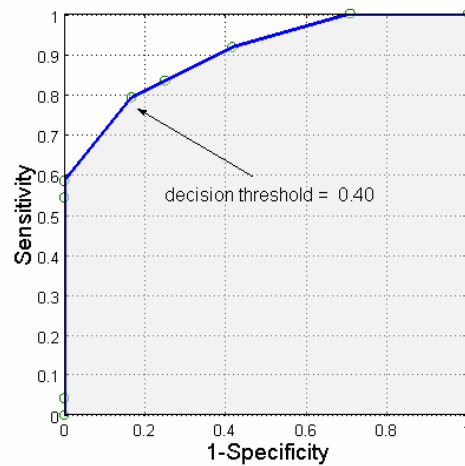


Fig. 6. ROC curve for the diagnostic algorithm. Decision threshold varied from 0.1 to 1 in 0.05 steps. Area under the curve is 0.90.

4. Discussion

The processes involved in acoustically induced blood stasis are neither simple nor straightforward and many physiological questions remain unanswered concerning the ultrasound-induced effects. Although the ultrasound intensities employed have been shown to create very little heating of the tissue and have not been shown to damage tissue, the effects of ultrasound on vessel diameter have yet to be addressed, i.e. does standing wave ultrasound constrict or dilate the vessels? High intensity traveling ultrasound waves have been shown by Dalecki to exert pressure on the walls of frog heart cavities¹⁷. The pressures required to cause banding in moving blood are much lower than the intensities needed to deform the tissue of the heart. The current experiments were designed to remain below tissue heating, tissue damage and tissue pressure thresholds.

Observed changes in oxy/deoxyhemoglobin concentration are believed to be caused by metabolic consumption of oxygen following slowing or cessation of blood flow in localized volumes of tissue. It is generally believed that tumor cells have higher metabolic rates and therefore consume more oxygen in relation to resting muscle. This alone would lead one to expect that oxyhemoglobin concentrations would drop faster in tumor tissue than in nontumor tissue. In general, such decreases were not observed in our experiment, although, in some instances tumor tissue did exhibit oxyhemoglobin drops when the optical probe was located in close proximity to visible (large) surface vessels. In these cases, higher initial oxyhemoglobin concentrations were also observed and the ultrasound-induced contrast was visible in the measured ratio signal. When the probe was moved to a location distant (1-2 mm) from the visible vessel, the initial oxyhemoglobin concentration dropped and the ultrasound induced contrast was much less pronounced. Notably, this contrast was much less dependent upon location in the nontumor leg.

The hypothesis of this experiment is that there are physiological and rheologic differences between healthy tissue and tumor tissue that could cause the tissues to respond differently to the presence of standing wave ultrasound. To study the physiological differences, immunohistochemical studies were conducted on the tumor and muscle tissue samples following imaging and cryostat sectioning. Fig. 7 illustrates total and perfused vessels in both tissue types following *i.v.* injection of a fluorescent perfusion marker (DiOC₇). From these images, total and perfused blood vessel area and spacing of the vessels were determined (Table 1). The immunohistochemistry data in Table 1 demonstrates that tumors display increased spacing of both total and perfused vessels (signifying reduced vascular densities) as well as a reduction in total and perfused vascular area (which indicates a decrease in overall blood volume).

Previous papers (eg. Ref. 18) have shown almost invariably that transplanted murine tumor models have reduced oxygen saturations when compared to surrounding normal tissue. This reduction of oxygen saturation is due primarily to

TABLE 1
IMMUNOHISTOCHEMISTRY RESULTS

Mouse #	Average Vessel Spacing	Percent Vessel Area	Ave. Perf. Vessel Spacing	Perc. Perf. Vessel Area
Tumor				
	Truncated			
16	25.00	4.88	68.74	1.12
17	27.08	4.25	34.37	4.07
18	29.16	3.34	49.99	1.10
19	22.91	4.69	31.25	3.13
20	20.83	6.01	58.32	1.63
21	25.00	5.14	49.99	1.69
22	29.16	4.51	43.74	1.66
23	33.33	4.21	45.83	2.16
Average	25.31	4.59	45.46	1.93
STD	4.29	0.67	11.22	0.73
Muscle				
16	8.33	16.21	12.50	8.98
17	8.33	17.48	12.50	7.61
18	6.25	19.68	14.58	6.03
19	10.42	16.76	10.42	18.54
20	10.42	15.23	25.00	2.67
21	10.42	14.85	12.50	9.94
22	10.42	15.59	12.50	4.36
23	12.50	12.82	14.58	8.99
Average	9.63	16.08	14.32	8.39
STD	1.91	2.02	4.51	4.80

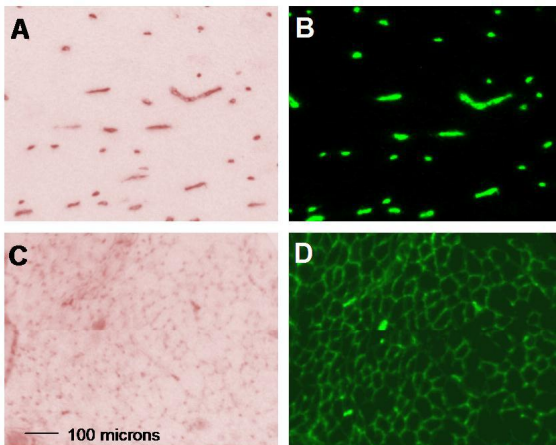


Fig. 7 Vessel stains in tumor (a) and muscle (c) tissue samples (transverse leg muscle). Perfused vessel stains in the same samples (b. and d.).

signal behaved in a manner similar to the muscular cases (i.e., substantial decreases in the signal were correlated to the ultrasound bursts).

The diagnostic algorithm demonstrated that it is possible to quantitatively differentiate tumor from muscle based on a single noninvasive measurement. It was found that for the decision threshold values of 0.40, the algorithm reached a specificity of 0.83 and a sensitivity of 0.79. As a measure of the algorithm accuracy, the initial assessment of the area under the ROC curve (by this experiment) was 0.90, suggesting that the constructed algorithm is a good classifier.

insufficiencies of the tumor vasculature to adequately supply oxygen. It was our hypothesis that, due to the tumor tissue tendency to have less blood, fewer vessels, and less oxygen saturation, the tumor will not have a large response to standing wave ultrasound when measured with optical spectroscopy.

Initial tumor and muscle tissue oxyhemoglobin concentrations varied from mouse to mouse, possibly due to the depth of the anesthesia. Comparison of the ultrasound-induced contrast of each leg to the opposite leg of the same mouse was implemented to reduce the mouse to mouse variance of oxyhemoglobin saturation. As noted in Ref. 11, there are potentially large differences in the diffuse reflectance spectra gathered from different mice and from various locations of a single tumor in each mouse.

For each mouse, the difference in ultrasound-induced oxyhemoglobin concentration changes between tumor and muscle tissue could result from differences in blood vessel counts and vessel orientation within the tissue, as well as differences in the metabolic rates of each tissue. The MCa-35 tumor is a highly vascularized, well perfused metastatic model and develops an extremely chaotic mesh of blood vessels. It is generally well oxygenated when compared to other tumor species models¹⁷. Alternative tumor models with lower oxygenation, fewer vessels, and decreased blood flow would be expected to show even less spectral contrast due to ultrasound.

In general, the ultrasound-induced contrast was much more pronounced when initial hemoglobin concentrations were elevated in both tissue samples. This elevation could be due to inflammation of the skin, higher vessel counts, large vessels in close proximity to the probe, less pressure exerted by the probe on the skin, etc. Although, experimental procedures were designed to decrease the effects of inflammation and probe force on the skin, it was unclear whether such factors led to the varying spectral responses between mice. Additional studies are needed to further investigate these factors.

Decreases in the observed I_{560}/I_{540} ratios were predictable and generally corresponded to the ultrasound bursts, but were not always easily observable. If the probe was positioned in the proximity of a major blood vessel in the tumor, the observed signal behaved in a manner similar to the muscular cases (i.e., substantial decreases in the signal were correlated to the ultrasound bursts).

5. Conclusions

The current study demonstrated that there were substantial and predictable ultrasound-induced changes in the I_{560}/I_{540} ratio signal obtained through *in vivo* spectroscopic measurements of diffuse light reflected from tumor and nontumor mouse tissue. The ratio signal is better correlated to the ultrasound signal for muscle tissue than tumor tissue and appears highly promising for noninvasive tissue diagnostics.

Acknowledgements

This work was supported by the U.S. National Institutes of Health Grant No. CA107860 awarded by the National Cancer Institute.

References

1. M. Dyson, B. Woodward, and J.B. Pond, "The flow of red blood cells stopped by ultrasound," *Nature* **232**, 572-573 (1971).
2. G. ter Haar and S.J. Wyard, "Blood cell banding in ultrasonic standing wave fields: a physical analysis," *Ultrasound Med. Biol.* **4**, 111-123 (1978).
3. W.L. Nyborg, "Microsonation of cells under near-threshold conditions," *Proc. 2nd World Congress of Ultrasonics Med.*, 360-366 (American Elsevier, New York, 1974).
4. G. ter Haar and M. Dyson, "Effects of ultrasound on circulation," *Biorheology* **4**, 207 (1977).
5. G. ter Haar, M. Dyson, and S.P. Smith, "Ultrastructural changes in the mouse uterus brought about by ultrasonic irradiation at therapeutic intensities in standing wave fields," *Ultrasound Med. Biol.* **5**, 167-179 (1979).
6. B.S. Brown, "How safe is diagnostic ultrasonography," *Canadian Med. Assoc. Jour.* **131**, 307-311 (1984).
7. W.L. Nyborg, "Biological effects of ultrasound: development of safety guidelines. Part II: General Review," *Ultrasound Med. Biol.* **27**, 301-333 (2001).
8. W.G. Zijlstra, A. Buursma and W.P. Meeuwssen-van der Roest, "Absorption spectra of human fetal and adult oxyhemoglobin de-oxyhemoglobin, carboxyhemoglobin and methemoglobin," *Clin. Chem.* **37**, 1633-1638 (1991).
9. T.J. Farrell, M.S. Patterson, and B.C. Wilson, "A diffusion theory model of spatially resolved, steady-state diffuse reflectance for the noninvasive determination of tissue optical properties *in vivo*," *Med. Phys.* **19**, 879-888 (1992).
10. E.L. Hull and T.H. Foster, "Steady-state reflectance spectroscopy in the P_3 approximation," *J. Opt. Soc. Am. A.* **18**, 584-599 (2001).
11. J.C. Finlay and T.H. Foster, "Hemoglobin oxygen saturations in phantoms and *in vivo* from measurements of steady-state diffuse reflectance at a single, short source-detector separation," *Med. Phys.* **31**, 1949-1959 (2004).
12. K. Yosioka, Y. Kawasima, "Acoustic radiation pressure on a compressible sphere," *Acoustica* **5**, 167-173, (1955).
13. B.M. Fenton, S.F. Paoni, J. Lee, C.J. Koch, and E.M. Lord, "Quantification of tumor vascular development and hypoxia by immunohistochemical staining and HbO_2 saturation measurements," *Br J Cancer* **79**, 464-471 (1999).
14. B.M. Fenton, S.F. Paoni, B.K. Beauchamp, and I. Ding, "Zonal image analysis of tumour vascular perfusion, hypoxia, and necrosis," *Br J Cancer* **86**, 1831-1836 (2002).
15. S. A. Prahl "Optical properties of hemoglobin," <http://omlc.ogi.edu/spectra/hemoglobin/summary.html> (1999).
16. V. Misic, B. A. Winey, B. Fenton, S. Paoni, L. Liao, P. Okunieff, H. Liu, K.J. Parker, Y. Yu, "Tumor detection *in vivo* with optical spectroscopy." *Proc. of the EMB 27th Annual Conf. Shanghai, (September 1-4, 2005).*
17. D. Dalecki, C.H. Raeman, S.Z. Child, and E.L. Cartensen, "Effects of pulsed ultrasound on the frog heart. 3. The radiation force mechanism," *Ultrasound Med. Biol.* **23**, 275-285 (1997).
18. B. M. Fenton, S. F. Paoni, B. G. Grimwood, and I. Ding, "Disparate effects of endostatin on tumor vascular perfusion and hypoxia in two murine mammary carcinomas," *Int.J Radiat.Oncol.Biol.Phys.* **57**, 1038-1046 (2003).

* bwiney@pas.rochester.edu ; phone 1 585 273 4103; fax 1 585 275 1531; www.pas.rochester.edu